POLITECNICO DI MILANO

Facoltà di Ingegneria Industriale

Corso di Laurea Specialistica in Ingegneria Aeronautica

Innovative Solid Fuels

for Hybrid Rocket Propulsion

Relatore: Luciano Galfetti

Tesi di Laurea di:

Mohamad Khattab 734231

ANNO ACCADEMICO 2010-2011

Abstract

Hybrid propulsion display several advantages over solid and liquid propulsion. Among these, the most important are safety, thrust throttability, possibility of engine re-start, low costs and low environmental impact. The main drawback of hybrid technology is its fuel low regression rate. The purpose of this work is to review the available literature on hybrid propulsion. Moreover, a comparison among different kinds of solid fuels was performed, in terms of average regression rate. The tested fuels are HTPB and paraffin wax. As expected from a literature review, paraffin-based solid fuels display higher regression rate when compared to that typical of HTPB-based fuels. This is due to the entrainment phenomenon that characterizes liquefying fuels, which form a liquid layer on their burning surface.

Table of Contents

Chapter 1

Motivations and objectives

1.1 Motivations

Hybrid rocket propulsion displays several advantages when compared to solid and liquid propulsion. The main advantages of the hybrid technology are the possibility of thrust modulation, restart and throttling capabilities, safe transportation and operation, low development and operational costs, and low environmental impact. On the other hand, low regression rate is the main drawback that has limited so far the full development of hybrid rocket technology.

The solid fuel regression rate is the rate at which the combustion front penetrates the solid grain and travels in the direction perpendicular to the grain surface. Many attempts have been made to increase the regression rate of the hybrid fuel, including for example addition of energetic ingredients (metal powders, metal hydrides), increase of convective thermal exchange coefficient through turbulence enhancement (swirled oxidizer injection), and use of liquefying fuels and exploitation of the entrainment phenomenon, i.e. the entrainment of droplets from the unstable liquid-gas interface, which can substantially increase fuel mass transfer leading to higher regression rates.

1.2 Objectives

The objective of the thesis is a review of the available literature on hybrid propulsion, focusing on history, main features and open problems related with this technology. Moreover, some firing tests were performed on an existing 2D hybrid facility. Pure HTPB and paraffin fuels were compared in terms of average regression rate.

1.3 Outline

Chapter 1 presents motivations, objectives and organization of the thesis.

Chapter 2 discusses the state of the art of hybrid rocket propulsion. This chapter deals with the historical background of the hybrid rocket propulsion, the main

features the hybrid rocket, the combustion process and combustion instability and the most common methods used to increase the regression rate of hybrid fuels.

Chapter 3 describes the experimental setup used for this work.

Chapter 4 presents the results of the experimental investigation.

In Chapter 5 the conclusion of this work are presented and future work is suggested.

Chapter 2

State of the art of Hybrid Rocket Propulsion

2.1 Historical Background

The early history of hybrid rocket development dates back to the early 1930s, at the same time when liquid and solid rockets development began.

Liquid propellant rockets could be stopped and restarted an unlimited number of times, and allow obtaining high specific impulse, but suffer from high system complexity and high costs. In a liquid propellant rocket, liquid oxidizer and liquid fuel are fed at high pressure to a combustion chamber where they mix and react producing high temperature, high pressure gases which exhaust through a converging-diverging nozzle producing thrust.
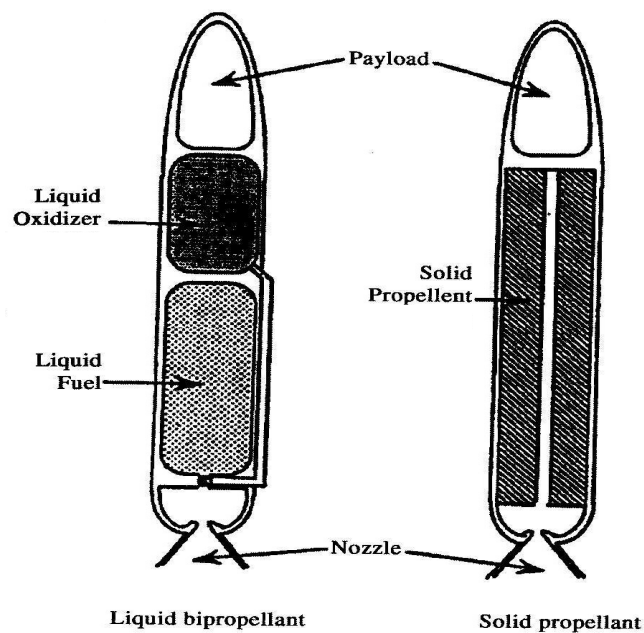
Figure 1 Liquid and Solid propellant rockets.

On the other hand, solid propellant rockets offer the advantage of simplicity, but give lower specific impulse and problems of safety and environmental impact. Solid propellant rocket doesn't require the complex and expensive machinery of liquid systems. However, in the solid propellant the solid fuel and oxidizer are mixed together producing an explosive fuel. Upon ignition the solid fuel burns

uninterrupted until all the fuel is exhausted. The liquid and solid propellant rockets are represented in figure 1.

Hybrid rocket engines display intermediate characteristics between solid rockets and liquid rockets; they are characterized by a phisical separation of fuel and oxidizer, the classical configuration being a solid fuel and a gaseous or liquid oxidizer. This separation between fuel and oxidizer results in intrinsic safety, stop-restart possibility, high theoretical performance and low costs. On the other hand, the diffusion flame consequent to the ingredients separation results in low regression rate values. Figure 2 represents the scheme of a hybrid rocket motor.
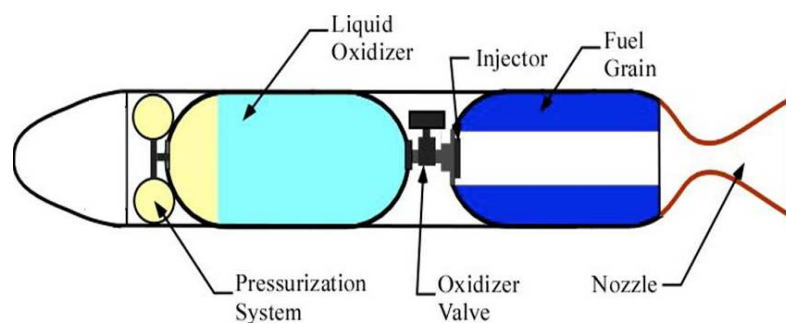
Figure 2 General configuration of a hybrid rocket motor.

The classical hybrid rocket configuration includes a solid fuel grain cast into the combustion chamber and a separate tank containing a liquid oxidizer. The oxidizer can be fed into the ports of the fuel grain in the combustion chamber either by gas pressure or by a pump system. The inverse hybrid motor includes a liquid fuel and a solid oxidizer. In the gas-generator type of hybrid rocket, the solid fuel is loaded with a small amount of solid oxidizer, forming a fuel-rich solid-propellant grain. Oxidizer is then injected into the after burner section to mix and burn with the fuel-rich gases generated by the solid grain. The combined type has both aspects of the classical and gas-generator types of hybrid motors because the oxidizer is injected into both the head end of the fuel grain and the aft mixing chamber.

Classical materials used as fuels in hybrid rockets are polymers such as hydroxyl terminated polybutadiene (HTPB). Higher regression rate fuels are obtained using liquefying fuels, such as paraffin and polyethylene waxes, which form a liquid layer on their burning surface. In this type of fuels the regression rate is generated by the vaporization of the liquid and the entrainment of liquid droplets into the gas stream. The entrainment mass transfer increases with deceasing viscosity and surface tension of the melt layer and increasing mass flux of the oxidizer. Typical oxidizers

are liquid oxygen, hydrogen peroxide, nitrogen tetroxide, and nitrous oxide. In a typical hybrid rocket motor the liquid oxidizer is injected axially into a pre-combustion chamber where it vaporizes then it passes through the ports of the fuel grain and reacts with fuel vapor. A post-combustion chamber ensures that all fuel and oxidizer are burnt before exiting the nozzle. Different types of hybrid rockets are shown in figure 3.
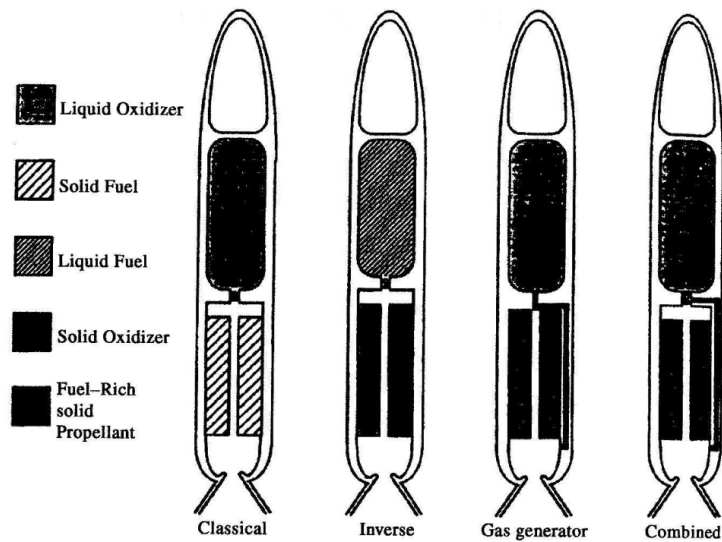
Figure 3 Various types of hybrid rockets.

2.2 Characteristics of Hybrid Rocket

As mentioned earlier, hybrid rocket technology displays several advantages when compared to liquid and solid propulsion. These features are discussed below.

1. Safety: since fuel and oxidizer are separated by distance and phase, hybrids have almost no explosion hazard and very few failure modes. Moreover, solid fuels are not hazardous for storage and transportation, unlike solid propellants and volatile liquid fuels such as hydrogen.

2. Insensitivity: unlike solid-propellant grains, where fuel and oxidizer are intimately mixed, hybrid-fuel grains are insensitive to cracks and imperfections. In conventional hybrids, heterogeneous reactions due to oxidizer attacking the fuel surface generally do not come into play because the diffusion flame zone shields the fuel surface from the oxidizer-rich core flow. Therefore, potential cracks and fuel imperfections that may increase the fuel surface area do not have a significant effect on the internal ballistics of the fuel grain.

3. Reliability: since only the oxidizer is stored in liquid form, hybrid rockets require only half the feed-system hardware needed by liquid rockets. This provides advantages in terms of improved reliability, lower feed system weight, and less complex mechanical design.

4. Energy management: hybrid rockets can be throttled for thrust control, maneuvering, motor shutdown, and restart by adjusting only the oxidizer flow rate while avoiding the necessity of matching hydraulic characteristics with the fuel, as must be done for liquid propellant rockets.

5. Fuel versatility: the solid-phase fuel provides a convenient matrix for introducing a variety of additives such as metal particles for high-energy missions.

6. Design flexibility: though most hybrid development efforts have focused on large boosters using the conventional configuration, hybrid motors can also be used for a variety of missions including in-space propulsion, satellite maneuvering, orbit maintenance, waste generators .

7. Environmental friendliness : hybrid rockets using typical propellants such as liquid oxygen (LOX) and rubber-base fuel such as HTPB, have environmentally clean exhaust without hydrogen chloride or aluminum oxide.

8. Low cost: hybrid rockets are very economical to both manufacture and launch because of their inherent safety and minimal failure modes.

Hybrid rockets also display some disadvantages with respect to liquid and solid rockets, as described below.

1. Slow regression rate: polymeric hybrid fuels, such as HTPB, regress rather slowly, generally at least an order of magnitude slower than solid propellants. To produce the necessary mass flow rate of pyrolyzed vapor from the fuel grain consistent with a desired thrust level, multiport grains with large wetted surface areas must be employed. Such grains require proportionally large pressure cases and can display poor volumetric loading.

2. Low volumetric loading: in addition to slow regression rates leading to poor volumetric loading, the use of aft combustion chambers downstream the fuel grain to complete the mixing and combustion of fuel and oxidizer further exacerbates the mass fraction disadvantage compared to liquid and solid systems.

3. Fuel residuals: conventional hybrid fuels with multiple ports cannot be burnt to completion because portions of the fuel web between the ports would

dislodge from the host grain and potentially block the nozzle. Therefore, a few percent of the fuel is left intact at the end of the mission.

4. Mixture ratio shift: because of the strong coupling between the oxidizer flow through the fuel port and the grain ballistic behavior, the overall mixture ratio during the combustion displays a time variation due to the increase in the port size. This variation affects the propulsion system performance. However, use of secondary oxidizer injectors and innovative grain designs can eliminate the mixture ratio shift.

5. Mixing/Combustion inefficiencies: hybrids have fundamentally different mixing and combustion processes than either liquid or solid propellant systems. In liquid engines, propellant mixing occurs on a droplet-size scale, whereas in solids the fuel and oxidizer are intimately mixed during the grain casting process. In hybrids, however, propellant mixing and combustion occur in a macroscopic diffusion flame zone that has a length scale of the same order as the fuel grain length. This model of mixing and combustion may result in slightly lower overall combustion efficiency than competing chemical systems.

2.3 Combustion Process

The combustion process occurring in a hybrid engine depends on the type of solid fuel used.

Figure 4 represents the flame structure of a hybrid rocket motor in the case of standard fuel. The oxidizer is injected in the axial direction while the fuel pyrolisis in the trasversal direction induces the so-called blowing effect.

The combustion takes place after ignition, when the gasified solid fuel and the injected liquid oxidizer mix and reach approximately the stoichiometric ratio. The flame is located within the dynamic boundary layer. This flame is diffusive and is controlled more by fluid-dynamics rather than by chemical kinetics. The combustion is sustained by the thermal energy feedback, by convection and radiation, from the diffusive flame to the burning surface of the solid grain. The combustion products are transported downstream by the convective flow and are expanded in the nozzle for thrust generation. The temperature grows from the wall temperature to the free stream temperature and has a maximum value in correspondence of the flame, whereas the speed grows monotonically from wall value to the free stream value.
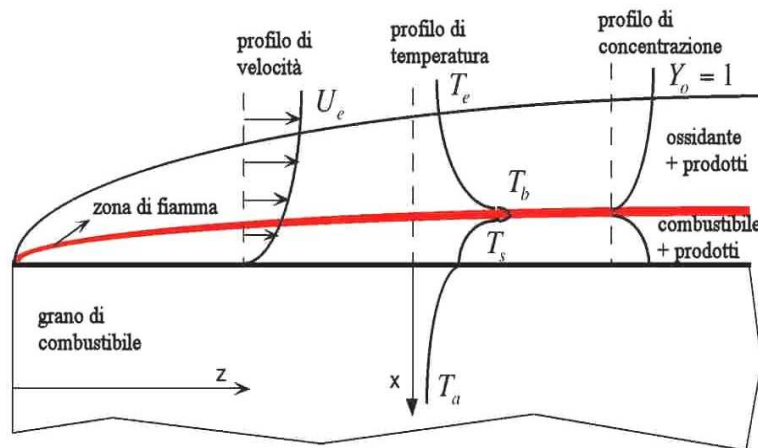
Figure 4 Hybrid propulsion flame structure.

Therefore, in a hybrid rocket combustion chamber the following processes take place (see figure 5):

1. thermal heating and pyrolysis of solid fuel;
2. desorption of polymer fragments from the pyrolyzing fuel surface;
3. diffusion of fragmented fuel species toward the flame zone;
4. formation of boundary-layer-like shear flow near surface regions of the solid-fuel grain;
5. diffusion of unburnt oxidizer to the pyrolyzing fuel surfaces and engagement in heterogeneous reactions;
6. propagation of the pyrolysis front spreading over exposed fuel surfaces;
7. fuel surface regression due to continue heating from the turbulent diffusion flame;
8. increase of axial mass flux along the port of the fuel grain due to mass addition;
9. acceleration of the bulk flow in the axial direction;
10. reduction of axial mass flux as port area increases in the later stage;
11. potential ejection of unburned sliver residues.

It can be therefore concluded that the combustion process occurring in a hybrid rocket engine (diffusion flame) is greatly different from that typical of a solid rocket motor (pre-mixed flame).
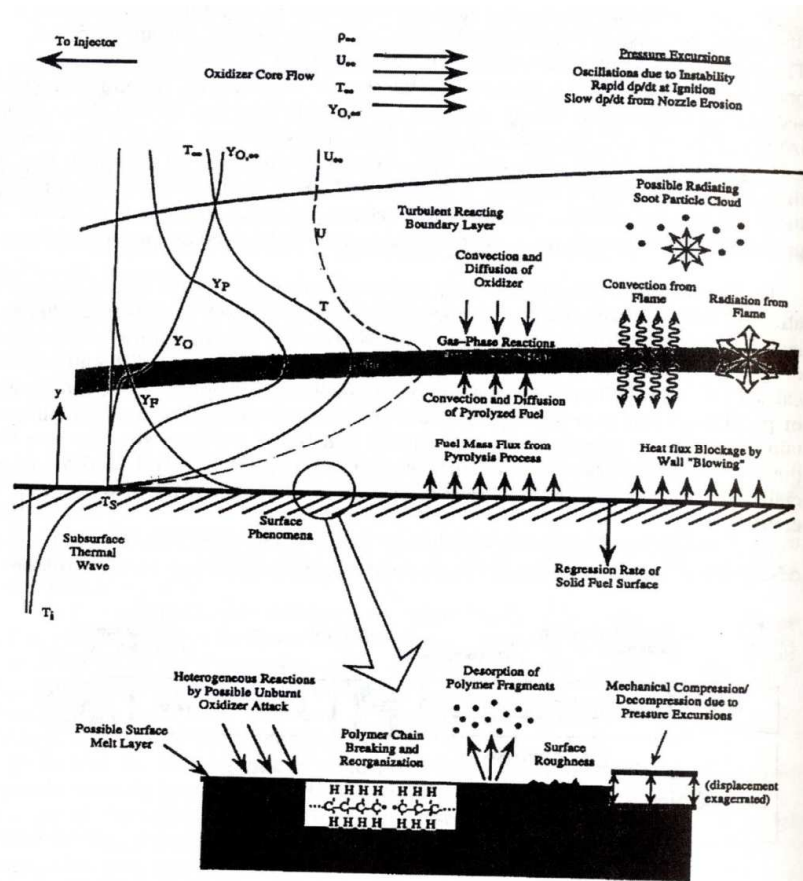
Figure 5 Physical processes involved in hybrid rocket combustion.

One of the physical phenomena that limits the burning rate in a hybrid motor is the so-called blocking effect that is caused by the high velocity injection of the vaporizing fuel into the gas stream. This difference in the combustion scheme of a hybrid motor significantly alters the burning rate characteristics compared to a solid rocket. Blocking can be explained as follows: increasing the heat transfer to the fuel causes the evaporative mass transfer from the liquid-gas interface to increase, but the increased blowing from the surface reduces the temperature and the velocity gradient at the surface thus reducing the convective heat transfer. The blowing also thickens the boundary layer and displaces the flame sheet further from the fuel surface leading to a further reduction in convective heat transfer. The position of the flame sheet and the shape of the thermal and velocity boundary layer is the result of a complex chemical and fluid-mechanical balance among the oxidizer flow entering the port, the fuel flow produced by evaporation and the flow of combustion products. As a result, the burning rate is limited in a fundamental way which is difficult to overcome by either increasing heat transfer to the fuel or by a reduction in the fuel heat of gasification. Although radiative heat transfer from

flame does not suffer from the blocking effect it is usually small compared to the convective heat transfer.

2.4 Methods for Regression Rate Increase

There are a lot of methods used to increase the regression rate of solid fuels. These methods include:

1. The use of energetic additives: a chemical approach used to increase the regression rate consists of adding high energy-fuel ingredients (such as metals and metal hydrides) to the solid fuel grain. The enhanced heat release near the regression surface increases the heat feedback and thus the regression rate of the solid grain.
2. Turbulence generators: another method for regression rate increase is the fluid-dynamic approach. A variety of devices or configurations can be used to generate a high level of turbulence at the regression surface, thus increasing the heat exchange. A possible technique involves the a screen of metallic wires inserted in the solid grain; during combustion the irregular edges of the screen act as turbulence initiators resulting in an increase of the overall regression rate. A cheaper alternative is to add an easily vaporizable component that during combustion creates a rough regression surface; this technique can be augmented by using crystalline additives to make the exposed surface even rougher.
3. Droplet entrainment: this technique is based on the use of fuels forming a thin liquid layer on their regression surface, allowing liquid droplets to be entrained by the gaseous oxidizer flow. If the liquid layer has enough low viscosity and low surface tension, under the action of a strong gaseous flow the liquid layer becomes unstable and gives rise to droplets that are expelled from the regression surface, thus greatly increasing the overall fuel mass transfer rate. Fuels of this kind include paraffin waxes, polyethylene waxes, and cryogenic substances that crystallize when solidify and appear very fluid when melt.

2.5 Combustion Instability

The hybrid combustion process tends to produce somewhat rougher pressure versus time characteristics than either liquid or solid rocket engines. However, a well-designed hybrid will typically limit combustion roughness to approximately 2 to

3% of mean chamber pressure. In any combustion device, pressure fluctuations tend to organize themselves around the natural acoustic frequencies of the combustion chamber or oxidizer feed system. When pressure oscillations occurr in hybrid motors, they have been observed to grow to a limited amplitude, which is dependent on oxidizer feed system and injector characteristics, fuel grain geometry characteristics, mean chamber pressure level, and oxidizer mass velocity.

Hybrid motors have two basic types of instabilities: oxidizer feed system-induced instability (non-acoustic), and flame holding instability (acoustic). Oxidizer feed system instability is essentially a chugging type and arises when the feed system is sufficiently soft. In cryogenic systems, this implies a high level of compressibility from sources such as vapor cavities or two-phase flow in feed lines combined with insufficient isolation from motor combustion processes. Flame-holding instabilities arise due to inadequate flame stabilization in the boundary layer and are not associated with feed system flow perturbations.
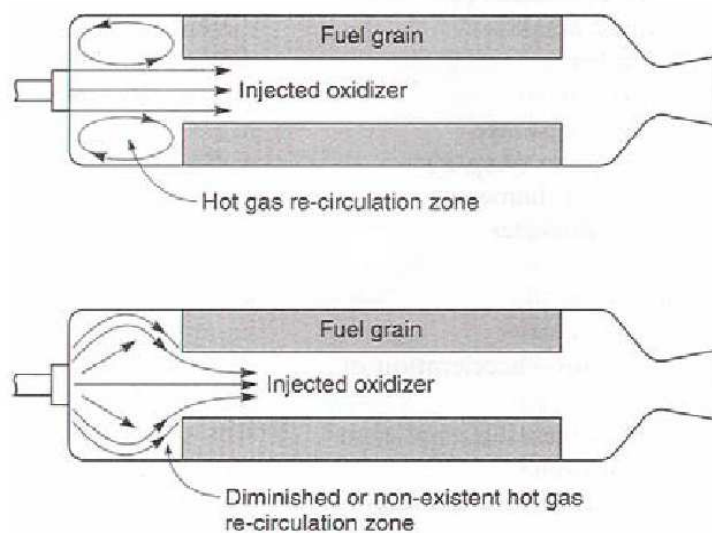
Figure 6 Axial and conical injection of oxidizer.

Flame-holding instabilities can be eliminated by several means, all of which act to stabilize combustion in the boundary layer. The first method is to use a pilot flame derived from injection of a combustible fluid such as hydrogen or propane to provide sufficient oxidizer preheating in the leading edge region of the boundary layer flame zone. With this technique, motor stability characteristics are relatively insensitive to the nature of the injector flow field. A second method involves changing the injector flow field to ensure that a sufficiently large hot gas recirculation zone is present at the head end of the fuel grain. Such a zone can be

created by forcing the upstream flow over a rearward-facing step or by strong axial injection of oxidizer (see figure 6).

Axial injection of oxidizer results in a strong hot gas flow recirculation zone at the fuel grain leading edge, producing a stable combustion. Whereas conical injection of oxidizer can produce a weak or nonexistent hot gas flow recirculation zone at the fuel grain leading edge, resulting in unstable combustion.

2.6 Pressure and Mixture Ratio vs. Time

Considering a zero dimensional combustion chamber and combustion gases composed of a mixture of perfect gases, the following mass balance equation can be written:

$$\frac{\partial(\rho_c V_c)}{\partial t} = \dot{m}_{in} - \dot{m}_{out}$$

where $\dot{m}_{in}$ is the inlet mass flow rate and $\dot{m}_{out}$ is the outlet mass flow rate through a supersonic gasdynamic nozzle. By making explicit all terms, one finds:

$$\frac{\partial(\rho_c V_c)}{\partial t} = \dot{m}_{ox} + \dot{m}_F - \frac{p_c A_t}{c^*}$$

Where $\dot{m}_{ox}$ is the mass flow rate of the liquid oxidizer and $\dot{m}_F$ is the mass flow rate of the gasified gaseous fuel.

$$\dot{m}_{ox} = \rho_{ox} u_{ox} A_{ox}, \qquad \dot{m}_F = \rho_F \dot{r}_F A_F$$

Under transient conditions it can be written:

$$\rho_c \frac{dV_c}{dt} + \frac{V_c}{\Gamma^2 c^{*2}} \frac{dp_c}{dt} = \dot{m}_{ox} + \rho_F \dot{r}_F A_F - \frac{p_c A_t}{c^*}$$

where the characteristic velocity c^* with frozen chemistry is:

$$c^* = \eta_{c^*} c_{th}^* = \eta_{c^*} \frac{1}{\Gamma} \sqrt{\frac{R}{M_c} T_c} = \eta_{c^*} \frac{\sqrt{\frac{R}{M_c} T_c}}{\sqrt{k\left(\frac{2}{k+1}\right)^{\frac{k+1}{k-1}}}}$$

Under steady conditions one finds:

$$p_c(t) = \frac{\eta_{c*} c_{th}^*}{A_t} [\dot{m}_{ox} + \rho_F r_F A_F]$$

Where A_F increase in time and r_F decrease in time.

Considering a combustion chamber made of a circular perforation of radius R and length L_p , it follows that:

- the fuel instantaneous regression rate decreases in time:

$$r_F(t) = a G_{ox}^n = a \left[\frac{\dot{m}_{ox}}{\pi R^2(t)} \right]^n$$

- the fuel instantaneous mass flow rate also varies in time:

$$\dot{m}_F(t) = \rho_F r_F A_F = 2\pi R(t) L_p \rho_F r_F(t)$$

$$= 2 a \pi^{1-n} L_p \rho_F \dot{m}_{ox}{}^n [R(t)]^{1-2n}$$

- the instantaneous pressure also varies in time:

$$p_c(t) = \frac{\eta_{c*} c_{th}^*}{A_t} \left[\dot{m}_{ox} + 2 a \pi^{1-n} L_p \rho_F \dot{m}_{ox}{}^n [R(t)]^{1-2n} \right]$$

- the instantaneous mass mixture ratio also varies in time:

$$\frac{O}{F} = \frac{\dot{m}_{ox}}{\dot{m}_F} = \frac{\dot{m}_{ox}{}^{1-n} [R(t)]^{-(1-2n)}}{2 a \pi^{1-n} L_p \rho_F} \approx \frac{\dot{m}_{ox}{}^{1-n}}{L_p [R(t)]^{1-2n}}$$

From these equations it can be concluded that the instantaneous pressure p_c and the instantaneous fuel mass flow rate $\dot{m}_F$ increase while the instantaneous mass mixture ratio O/F decreases in time for n<0.5; vice versa for n>0.5.

2.7 Classical Fuels

They are polymers such as HTPB (Hydroxyl-terminated polybutadiene). The regression rate of this kind of fuels rely solely on the evaporation of the solid fuel into the gas stream.

HTPB is a classical fuel used in hybrid propulsion because of its good physical properties and good performance. It is a polymer of butadiene terminated at each end with a hydroxyl functional group. It is a viscous liquid that become an elastic

solid when it reacts with another organic material (Isophorone diisocyanate, IPDI). HTPB has the following formula:

$HO-CH_2-CH=CH-CH_2-(CH_2-CH=CH-CH_2)_n-CH_2-CH=CH-CH_2-OH$
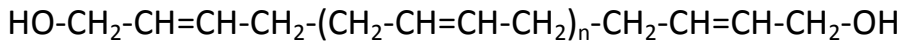
where n is the number of butadiene monomers presents in the polymer. The HTPB used in this work is HTPB R-45, composed of 45 monomers of butadiene and has the following properties:

- Molecular mass: 1200 g/mol;
- Density: 0.913 g/cm^3;
- Heat of combustion: 10^6 J/kg.

2.8 Advanced Fuels

These fuels such as paraffin and polyethylene waxes display a very high regression rate with respect to the traditional fuels. They produce a very thin, low viscosity, low surface tension liquid layer on their burning surface. The instability of this layer is driven by the oxidizer gas flow in the port and leads to entrainment of droplets into the gas stream greatly increasing the overall fuel mass transfer rate. This mechanism acts like a continuous spray injection system distributed along the port. Since droplet entrainment is not limited by diffusive heat transfer to the fuel from the combustion zone, this mechanism can lead to much higher surface regression rates than those typical of conventional polymeric fuels. In figure 7 the regression rate of paraffin-based fuels is compared to that of HTPB.
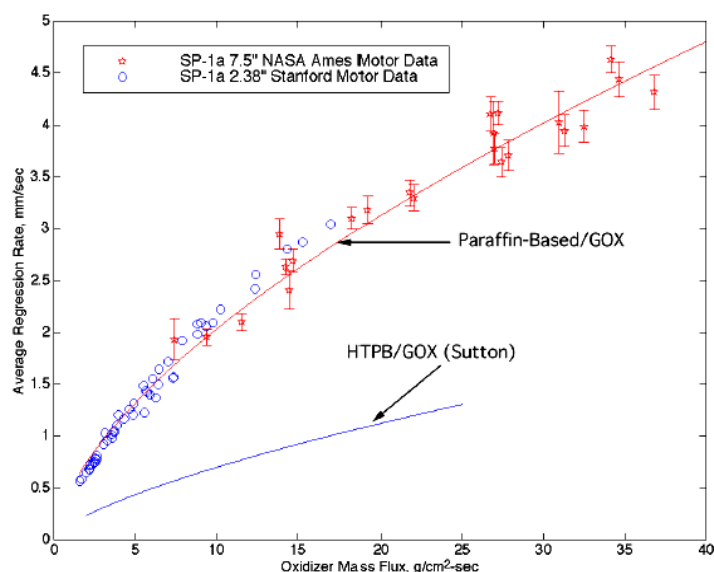
Figure 7 Regression rates vs. oxidizer flux for HTPB and paraffin-based fuels.

The entrainment mass transfer depends on the operational parameters (pressure, oxidizer flux) and on the material properties of the solid fuel (viscosity, surface tension). The entrainment mechanism is represented in figure 8.
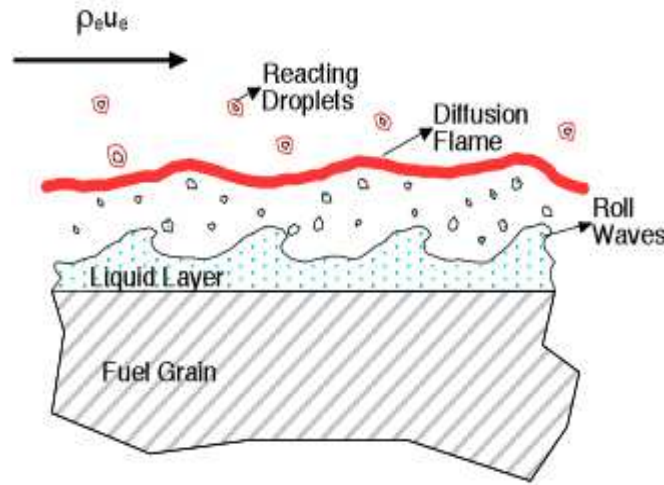
Figure 8 Entrainment of liquid droplets into the gas stream.

The entrainment mass transfer has the following expression:

$$\dot{m}_{ent} \propto \frac{P_d^{\alpha} h^{\beta}}{\mu_l^{\gamma} \sigma^{\pi}}$$

The experimental data suggested that the dynamic pressure exponent is in the range of 1-1.5. For example Gater and L'Ecuyer scaling for large mass fluxes indicates that α is approximately 1.5 and β is equal to 2. The viscosity and surface tension exponents are both predicted to be 1.

The advantages of liquefying fuels can be summarized as follows:

- Regression rate is 3-5 times as high as the classic polymeric fuels.
- The fuel is non-toxic, non-hazardous and environmentally friendly: the products of combustion are carbon dioxide and water.
- Paraffin-based fuels are inexpensive, typically one to two orders of magnitude less than solid propellants.
- Processing of the fuel grains is simple: no polymerization reactions are involved and no curing agents are required.
- Paraffin waxes are hydrophobic, making them an ideal binder for metal, metal hydride or dense organic additives.
- Being inert, paraffin based fuels effectively have an infinite storage life.

2.9 Derivation of Hybrid Fuel Regression Rate Equation for Classical fuels

Figure 9 represents the energy balance at the fuel grain surface. The general steady-state energy balance can be written as follows:

Energy input fuel surface = Energy output of fuel surface

$Q_{convection}$ + $Q_{radiation\ in}$ = $Q_{conduction\ in}$ + $Q_{phase\ change}$ + $Q_{radiation\ out}$
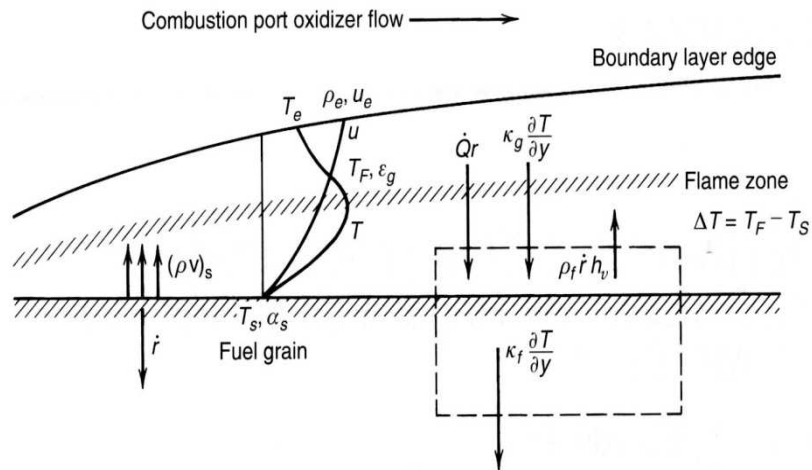
Figure 9 Energy balance at fuel grain surface.

Neglecting radiation and in depth conduction in the fuel mass, the steady state surface energy balance becomes:

$$\dot{Q}_c = \rho_f \dot{r} h_v$$

where $\dot{Q}_c$ is the energy transferred to the fuel surface by convection, and ρ_f, $\dot{r}$, and h_v are respectively the solid fuel density, surface regression rate, and overall fuel heat of vaporization or decomposition. At the fuel surface the heat transferred by convection equals that transferred by conduction so that:

$$\dot{Q}_s = h\Delta T = k_g \left.\frac{\partial T}{\partial y}\right|_{y=0}$$

where h is the convective heat transfer film coefficient, ΔT is the temperature difference between the flame zone and the fuel surface, k_g is the gas phase conductivity, and $\left.\frac{\partial T}{\partial y}\right|_{y=0}$ is the local boundary layer temperature gradient evaluated at the fuel surface. The central problem in determining the hybrid fuel regression rate is thereby reduced to determining the basic aerothermal properties

of the boundary layer. The heat transfer coefficient at the wall is related to the skin friction coefficient via the following relationship:

$$C_h = \frac{C_f}{2} Pr^{-2/3}$$

where C_f is the skin friction coefficient with blowing, C_h is the Stanton number, and Pr is the Prandtl number. Furthermore, the Stanton number can be written in terms of the heat flux to the fuel surface as:

$$C_h = \frac{\dot{Q}_s}{\Delta h \rho_e u_e}$$

where Δh is the enthalpy difference between the flame zone and the fuel surface, and ρ_e, u_e are the density and velocity of oxidizer at the edge of the boundary layer. Combining the equations, the regression rate of the fuel surface can be written as:

$$\dot{r} = \frac{C_f}{2} \frac{\Delta h}{h_v} \frac{\rho_e u_e}{\rho_f} Pr^{-2/3}$$

From boundary layer theory, one can show that the skin friction coefficient without blowing (C_{f0}) is related to the local Reynolds number by the relation:

$$C_{f0} = 0.0296 Re_x^{-0.2} \qquad (5x10^5 \leq Re_x \leq 1x10^7)$$

Experiments have shown that C_f is related to C_{f0} by the following relation:

$$\frac{C_f}{C_{f0}} = 1.27\beta^{-0.77} \qquad (5 \leq \beta \leq 100)$$

where the blowing coefficient β is defined as:

$$\beta = \frac{(\rho v)_s}{\rho_e u_e C_f/2}$$

Figure 10 represents the blocking factor C_f/C_{f0} in function of the blowing coefficient β.

In a turbulent boundary layer, the prandtl number is very nearly equal to 1. It can be shown that for Pr=1, β as defined in the previous equation, is also equal to $\Delta h/h_v$. Noting that $\rho_e u_e$ is the definition of oxidizer mass velocity (G), the equation that express the regression rate can be written in the final form as:

$$\dot{r} = 0.036 \frac{G^{0.8}}{\rho_f} \left(\frac{\mu}{x}\right)^{0.2} \beta^{0.23}$$

The coefficient 0.036 is applied when the quantities are expressed in the English Engineering system of units.
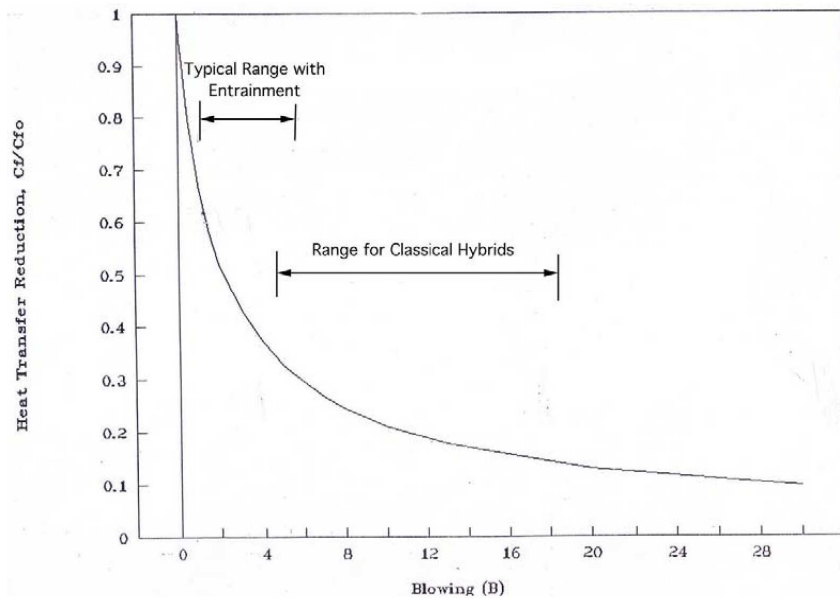
Figure 10 Blocking factor C_f/C_{f0} in function of blowing coefficient β

In some hybrid motors, radiation may be a significant contributor to the total fuel surface heat flux. Such motors include those with metal additives to the fuel grain (such as aluminum) or motors in which soot may be present in significant concentrations in the combustion chamber. In these instances the regression rate equation must be modified to account for heat flux from a radiating particle cloud. The radiative contribution affects surface blowing, and hence the convective heat flux as well. In this case the total heat flux to the fuel surface is expressed by:

$$\dot{Q}_s = \rho_f \ddot{r} h_v = \dot{Q}_c e^{-\frac{\dot{Q}_{rad}}{\dot{Q}_c}} + \dot{Q}_{rad}$$

The radiation heat flux has been hypothesized to have the following form:

$$\dot{Q}_{rad} = \sigma \alpha T_F^4 (1 - e^{-ACz})$$

where the term $1 - e^{-ACz}$ is ε_g, the emissivity of particle-laden gas, σ is the Stefan-Boltzmann constant, α is the fuel surface absorptivity. The regression rate in the presence of radiation is expressed in function of the regression rate in the absence of radiation by the following relation:

$$\frac{\dot{r}}{\dot{r}_c} = e^{\left(-0.75 \frac{\dot{Q}_r}{\dot{Q}_c}\right)} + \frac{\dot{Q}_r}{\dot{Q}_c}$$

Where $\dot{r}$ and $\dot{r}_c$ are respectively the regression rate with and without radiation.

2.10 Derivation of Hybrid Fuel Regression Rate Equation for Advanced Fuels

The formation of liquid layer instabilities and entrainment of liquid droplets require three major modifications in the classical hybrid combustion theory:

1. The ratio of the enthalpy difference to the effective heat of gasification ($\Delta h/h_v$) that appears in the thermal blowing parameter expression is altered. The effective heat of gasification is reduced because the evaporation energy required for the fuel mass transfer from the surface is partly avoided by the mechanical entrainment of the liquid, whereas the enthalpy difference between the flame and the surface is also reduced because some of the reactants are now in liquid phase.

2. The blocking factor C_H/C_{H0} that modifies the convective heat flux to the surface is also altered as a result of the presence of the two-phase flow. The blocking factor can be expressed as a function of evaporation blowing parameter:

$$C_H/C_{H0} = f(B_g)$$

The evaporation blowing parameter B_g includes only the gaseous phase mass transfer from the fuel surface.

3. The ripples formed on the liquid layer surface increase the surface roughness and the heat transfer from the flame front to the surface.

In general, the total regression rate of a hybrid motor can be written as a sum of the evaporation regression rate that is generated by the vaporization of the liquid into the gas stream and the entrainment regression rate that is related to the mass transfer mechanically extracted from the liquid surface.

$$\dot{r} = \dot{r}_v + \dot{r}_{ent}$$

For an arbitrary combination of the entrainment and evaporative mass transfer, the energy balance at liquid gas interface is:

$$\dot{r}_v + \left[R_{he} + R_{hv} \left(\frac{\dot{r}_v}{\dot{r}} \right) \right] \dot{r}_{ent} = F_r \frac{0.03 \mu_g^{0.2}}{\rho_f} (1 + \frac{\dot{Q}_r}{\dot{Q}_c}) B \frac{C_H}{C_{H0}} G^{0.8} z^{-0.2}$$

where

$$R_{hv} = \frac{C_l \Delta T_1}{h_s + L_v}, \qquad R_{hs} = \frac{h_m}{h_s + L_v}$$

The nondimensional energy parameters for entrainment R_{he} and vaporization R_{hv} are introduced because the material that is extracted through the entrainment mechanism possesses different heating histories (that is, no heat of vaporization is required for entrainment). The assumption is made that the effective heating in the liquid phase required for fuel material, which is going through the entrainment mass transfer mechanism, reduces linearly as the vaporization component of the regression rate decreases.

The roughness parameter Fr is introduced in the energy equation to account for the increased heat transfer by wrinkling of the liquid surface. It has been argued by Gater and L'Ecuyer that the surface roughness decreases with increasing dynamic pressure of the gas flow. The empirical formula for the roughness correction parameter suggested by Gater and L'Ecuyer can be expressed in terms of the operational parameters of the motor as:

$$F_r = 1 + \frac{14.1 \rho_g^{0.4}}{G^{0.8}(T_g/T_v)^{0.2}}$$

The expression of the blowing correction C_H/C_{H0} given by Marxman:

$$\frac{C_H}{C_{H0}} \cong \frac{2}{2 + 1.25 B_g^{0.75}} = \frac{C_{B1}}{C_{B1} + C_{B2}(\frac{\dot{r}_v}{\dot{r}_{cl}})^{0.75}}$$

These coefficients are defined as:

$$C_{B1} = \frac{2}{2 + 1.25 B^{0.75}}, \qquad C_{B2} = \frac{1.25 B^{0.75}}{2 + 1.25 B^{0.75}}$$

 The blowing correction factor C_H/C_{H0} is represented in figure 11.

The classical regression rate can be written as:

$$\dot{r}_{cl} = \frac{0.03 \mu_g^{0.2}}{\rho_f}(1 + \frac{\dot{Q}_r}{\dot{Q}_c}) B C_{B1} G^{0.8} z^{-0.2}$$
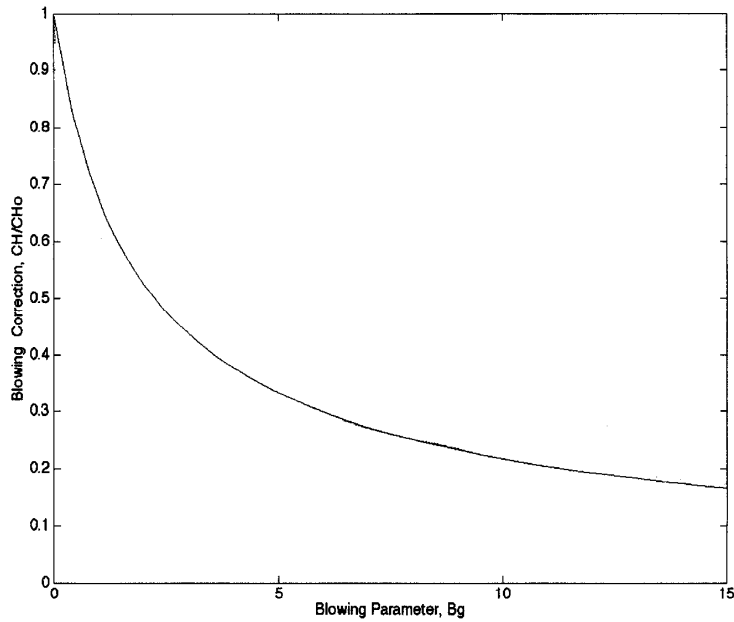
Figure 11 Blowing correction according to Marxman's formula.

The entrainment regression rate can be written as in terms of the mass flux in the port and the total regression rate as:

$$\dot{r}_{ent} = \alpha_{ent}\,\frac{G^{2\alpha}}{\dot{r}^{\beta}}$$

where a_{ent} is a function of the properties of the selected fuel and average gas density. For simplicity the assumption is made that this coefficient is constant for a given fuel.

By resolving this set of non linear algebraic equations the total regression rate as a function of the axial location and local mass flux can be obtained.

Chapter 3

Experimental Setup

3.1 General Layout

The experimental set up used for this work includes a combustion chamber, an oxidizer inlet system, a nitrogen inlet system and a pyrotechnic ignition device.

The combustion chamber is a 2D slab hybrid burner, available at SPLab, and is shown in Figure 12.
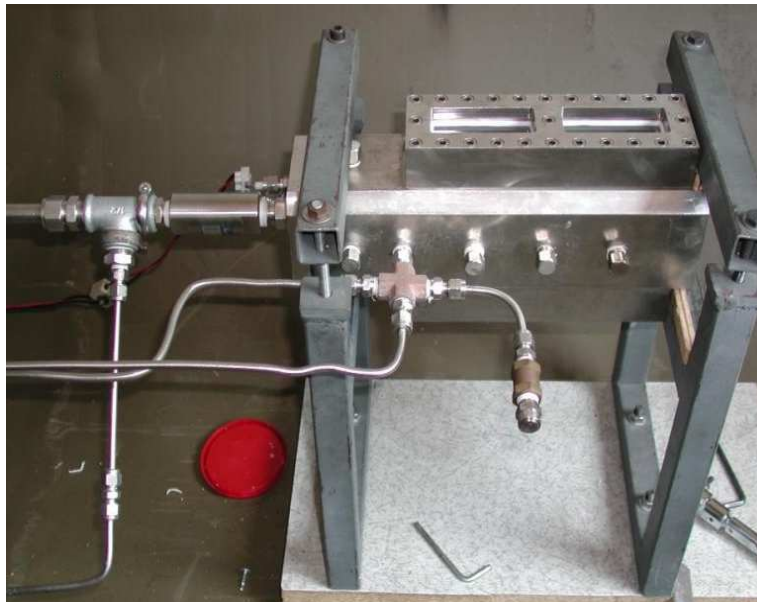
Figure 12 Combustion chamber.

Nitrogen is used as a cooling flow after combustion shutdown, with the aim to extinguish the oxidation reactions in the combustion chamber.

Pyrotechnic igniters are characterized by a metalized solid propellant charge, that burns by the contact with an electric wire that is heated by joule effect. The hot gases generated from the combustion of the main charge heat the surface of the solid fuel grain, and the combustion begins when the oxidizer arrives to the combustion chamber.

A single slab grain is shown in Figure 13.
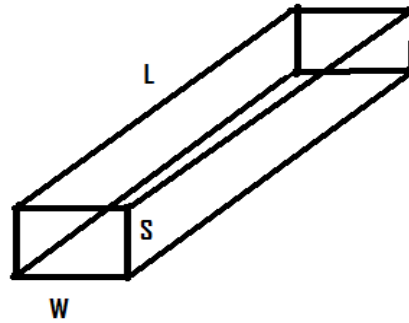
Figure 13 Single slab grain. Sample sizes: 50 x10 x5 mm.

3.2 Flow Rate and Pressure measurements

The basic principle used to measure the flow rate is that when a fluid stream is restricted, its pressure decreases by an amount which depends on the rate of flow through the restriction. Therefore, the pressure difference between points before and after the restriction can be used to indicate flow rate. Several devices are used to measure the flow rate, the most common devices are the venturi tube, the flow nozzle, the orifice, and the flow tube. The derivation of the relationship between the pressure difference and the volume flow rate is the same regardless of which type of device is used. An orifice plate is used to measure the flow rate.

An orifice plate is a restriction with an opening smaller than the pipe diameter which is inserted in the pipe; the typical orifice plat has a concentric, sharp edged opening, as shown in Figure 14. Because of the smaller area the fluid velocity increases, causing a corresponding decrease in pressure. The flow rate can be calculated from the measured pressure drop across the orifice plate. The orifice plate is the most commonly used flow sensor, but it creates a rather large non-recoverable pressure due to the turbulence around the plate, leading to high energy consumption .The pressure difference before and after the orifice plate is measured by a differential manometer.

The volume flow rate is determined using this formula:

$$Q = CA_0 \sqrt{\frac{2\Delta p}{\rho}}$$

 where C is the discharge coefficient that is a function on the Reynolds number of the flow (see figure 14), ρ is the fluid density, A_0 is the area of the orifice hole, and Δp is the pressure difference before and after the orifice.

The Reynolds number is determined by this formula:

$$N_R = \frac{\rho V D}{\mu}$$

Where V is the velocity of the flow, D is the diameter of the pipe, and μ is the fluid dynamic viscosity.

The oxidizer mass flow rate can be determined multiplying the volume flow rate by the density of the fluid ($\dot{m} = \rho Q$).
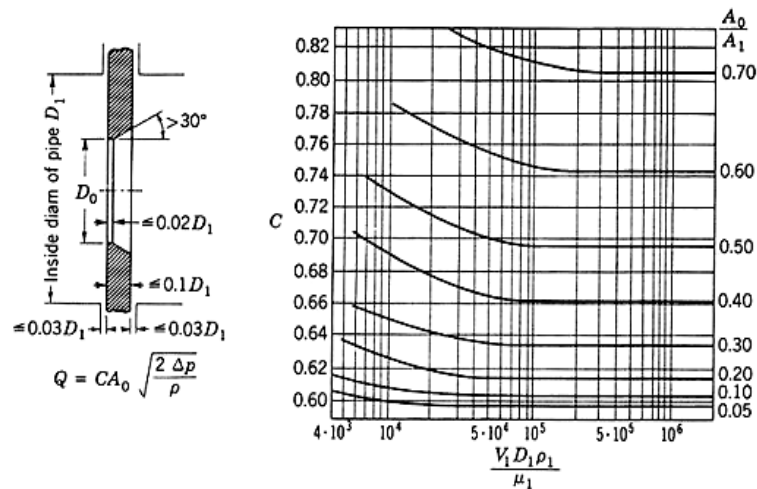
Figure 14 Discharge coefficient in function of the Reynolds number R_D.

The combustion chamber pressure is measured using a pressure transducer connected to a computer.

3.3 Regression Rate measurement

The average regression rate is determined as the ratio between the mass of the fuel consumed during combustion and the product of burning time, fuel density and fuel combustion area:

$$\dot{r}_f = \frac{\Delta m}{t_b \rho_f A_b},$$

where Δm is the burned fuel mass, ρ_f is the density of the solid fuel, t_b is the burning time and A_b is the burning surface.

Chapter 4

Results of the Experimental Investigation

Firing tests were performed in double slab fuel configuration, using pure oxygen as oxidizer, with operating pressure of 1.5 bar and oxygen mass flux ranging from 150 kg/m^{2}s to 350 kg/m^{2}s. Fuels tested include pure HTPB and paraffin.

The solid fuel regression rate can be expressed as a function of the oxidizer mass flux as:

$$\dot{r} = aG_{ox}^{n}$$

where:

G_{ox} is the oxidizer mass flux.

The constants a and n are obtained fitting the experimental data with a power law.

The values of these constants obtained for pure HTPB fuel are a=0.05 and n= 0.44.

For paraffin fuel, the coefficients a and n obtained are higher (a=0.061 and n=0.5437) than those obtained for HTPB. The relationship between the regression rate and the oxidizer mass flux for the paraffin wax is :

$$\dot{r} = 0.061G_{ox}^{0.5437}$$

Figure 15 shows a comparison between the regression rate of HTPB and paraffin wax in function of oxygen mass flux.
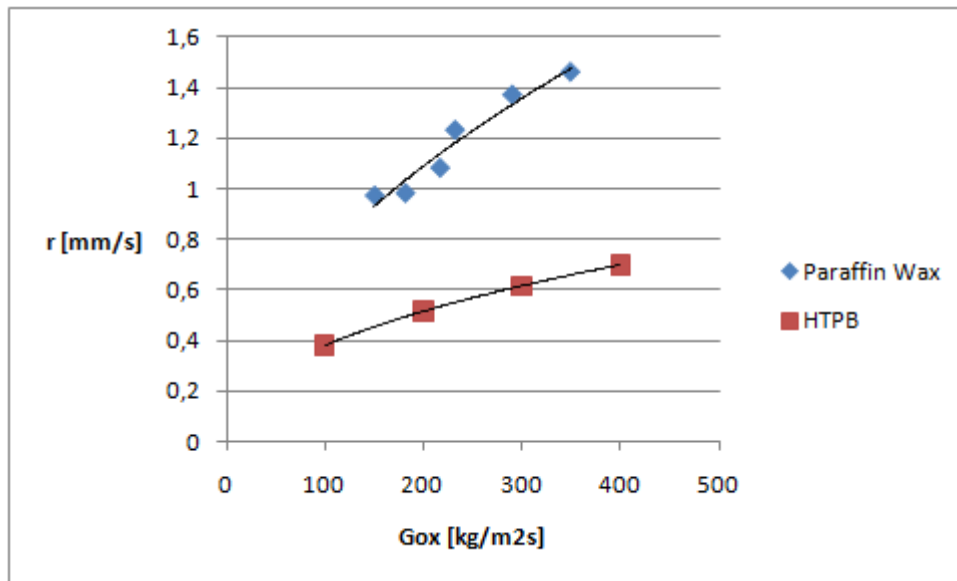
Figure 15 Regression rate of HTPB and paraffin wax in function of oxygen mass flux.

It can be observed that paraffin regression rate is higher than that of HTPB (+100% at 200 kg/m^{2}s). This is because in the case of paraffin wax the regression rate is the sum of the entrainment regression rate and the evaporation regression rate, while in the case of HTPB the regression rate depends only on evaporation. The entrainment of droplets by the gaseous oxidizer stream flowing in the port above the surface is the main reason for this increase of the regression rate.

Chapter 5

Conclusion and Future Work

In this work a survey of the available literature on hybrid propulsion was performed, focusing on historical background, main features of a hybrid rocket engine, methods for regression rate increase, combustion instability. Attention was also focused on the differences between standard and innovative fuels, and their respective combustion processes. Some firing tests were then performed in order to compare HTPB and paraffin fuels in terms of average regression rate. Paraffin fuel use results in a regression rate increase of 100% with respect to HTPB, at the selected oxygen mass flux. The higher regression rate values displayed by paraffin are due to its higher tendency to entrainment phenomenon.

Some future developments can be suggested:

- Measurement of the instantaneous regression rate using resistive probes.
- Measurement of the temperature in the combustion chamber in order to estimate the quality of the combustion process.
- Analysis of the mechanical properties of the paraffin based fuel in order to obtain a complete characterization ballistic-mechanic of this class of advanced fuels.

Nomenclature

$\dot{r}$ = regression rate, mm/s

μ_g = viscosity of gas, milliPa-s

ρ = density kg/m^3

$\dot{Q}_r$ = radiative heat transfer at the surface, kJ/m^2-s

$\dot{Q}_c$ = convective heat transfer at the surface, kJ/m^2-s

B = blowing parameter

B_g = evaporation blowing parameter

F_r = heat-transfer correction factor for surface roughness

h = melt layer thickness, mm

G = mass flux of oxidizer, kg/m^2-s

z = axial distance along the port, m

σ = surface tension, milliN/m

P_d = dynamic pressure in the port, Pa

t_b = burning time, s

μ = viscosity, milliPa-s

C_H = Stanton number with blowing

C_{H0} = Stanton number without blowing

C_{B1}, C_{B2} = blowing correction coefficients

C_f, C_{f0} = skin friction coefficients with and without blowing

Δh = enthalpy difference between the flame and the surfaces, kJ

k, ratio of specific heats (c_p/c_v)

R = the gas constant [J/Kg K]

Pr = Prandtl number

Re = Reynlods number

h_m, h_e = total heats of melting and entrainment, kJ/Kg

L_m, L_v = latent heat of melting and vaporization, kJ/kg

T_g = average gas phase temperature, K

T_m, T_v = melting and vaporization temperature, K

ΔT_1 = temperature difference, T_v-T_m, K

R_h = ratio of effective heats of gasification for entrainment and vaporization

C = specific heat kJ/kg-s

c^* = characteristic velocity, m/s

η_{c*} = efficiency of the characteristic velocity

C_f = skin-friction coefficient

α,β = dynamic pressure and thickness exponents

A_t = nozzle throat area, m^2

P_c = combustion chamber pressure, pa

T_c = combustion chamber temperature, K

M_c = average molar mass of combustion products, kg/kmol

$\dot{m}_{ox}$ = oxidizer mass flow rate, kg/s

$\dot{m}_F$ = fuel mass flow rate, kg/s

$\dot{m}_{ent}$ = entrainment mass flux from fuel surface, kg/m^2-s

Q = volume flow rate, m^3/s

$\dot{m}$ = mass flow rate, kg/s

A_0 = area of the orifice hole, m^2

C = Discharge coefficient

A_b = combustion area, mm^2

Subscripts

ent = entrainment

g = gas

l = liquid

s= solid

v = vaporization

f = fuel

References

[1] G.P. Sutton, Rocket Propulsion Elements, Wiley, New York, USA, 6th edition, 1992.

[2] L.T. De Luca, Problemi energetici in propulsione aerospaziale, Politecnico di Milano, Prima Edizione, 1997.

[3] M.A. Karabeyoglu, D. Altman and B.J. Cantwell, Combustion of Liquefying Hybrid Propellants: part 1, General Theory, Journal of Propulsion and Power, 18(3): 610-620, 2002.

[4] Martin J. Chiaverini, Kenneth K. Kuo, Fundamentals of Hybrid Rocket Combustion and Propulsion, Vol.218, 2006.

[5]   R.A. Gater, and M.R.L. L'Ecuyer, A Fundamental Investigation of the Phenomena that Characterize Liquid Film Cooling, International Journal of Heat and Mass Transfer, 13(3):1925-1939, 1970.